Electrochemical corrosion behavior of biomedical Ti–22Nb and Ti–22Nb–6Zr alloys in saline medium

B. L. Wang, Y. F. Zheng* and L. C. Zhao

The aims of this study were to investigate the effects of Zr addition and potentiodynamic polarization on the microstructure and corrosion resistance of Ti–22Nb and Ti–22Nb–6Zr alloy samples. The corrosion tests were carried out in 0.9% NaCl at 37 °C and neutral pH value, utilizing the OCP, potentiodynamic polarization, and electrochemical impedance spectroscopy (EIS) techniques. The results of XRD and optical microscopy indicated that the addition of Zr stabilized the β phase, which plays a crucial role in the corrosion resistance improvement of the Ti–22Nb–6Zr alloy. From the polarization curves, it can be seen that the alloys exhibited a wide passive region without the breakdown of the passive films and also low corrosion current densities. In addition, the values of the corrosion current densities and passive current densities decreased with the addition of 6 at% Zr into the Ti–22Nb alloy. The EIS results of these two alloy samples after 1-h immersion in 0.9% NaCl solution, and being fitted by $R_S(Q_P R_P)$ model, suggested that the corrosion resistance of the passive films improved with the addition of Zr and only a single passive film formed on the surfaces. However, two time constants were observed for the Ti–22Nb and Ti–22Nb–6Zr alloy samples after potentiodynamic polarization, the spectra of which can be fitted using the $R_s(Q_o(R_o(Q_b R_b)))$ model. In addition, the corrosion resistance of the two alloy samples was reinforced significantly because of polarization when compared to the immersed samples. All these observations suggested a nobler electrochemical behavior of the titanium alloys with the addition of Zr element and after polarization.

1 Introduction

Titanium and its alloys are one of the most widely studied and used metallic biomaterials, particularly those with vanadium- and aluminum-free Ti alloys, since these elements exhibit high cytotoxicity and negative tissue response in vivo and may induce senile dementia, neurological disorders, and allergic reactions [1–4]. It is well known that the recent metallic biomaterials research has focused on the β-type titanium alloys with excellent biocompatibility and low elastic modulus. The former advantage provides a biological acceptance for the implant in human body and the latter promotes an appropriate load sharing between implant and the surrounding hard tissue [5, 6]. In the last decade, Nb, Ta, Zr, Mo, and Sn, which are judged to be non-toxic and non-allergic, and are considered excellent β-stabilizing elements have

B. L. Wang, Y. F. Zheng, L. C. Zhao
School of Materials Science and Engineering, Harbin Institute of Technology, Harbin 150001 (P. R. China)
E-mail: yfzheng@hit.edu.cn

been selected as safe alloying elements to Ti alloys [7–11]. To determine the suitability of a material for implant application, several properties of implants must be evaluated. One of the most important aspects is the corrosion behavior because the ions releasing from the metallic implant to the surrounding tissues may give rise to biocompatibility problems [12]. Its studies in vivo and in vitro under simulated human body environment are well reported.

The Ti–Nb alloys have presented superior corrosion resistance when compared to the traditional Ti–6Al–4V alloy [13]. A uniformly passive film consisted of Ti_2O_3, TiO_2, and Nb_2O_5 can be formed on the surface of the Ti–Nb alloys [14, 15]. *Mareci* et al. [16] compared the electrochemical corrosion behaviors of CP Ti, Ti–6Al–4V, Ti–5Al–2.5Fe, Ti–6Al–7Nb, and Ti–6Al–2Nb–1Ta–1Mo alloys in artificial saliva. Their results indicated that the corrosion behavior of Ti–6Al–4V alloy was not affected on substituting vanadium with niobium, iron, molybdenum, and tantalum. *Tamilselvi* et al. [17] have recently reported the Ti–6Al–7Nb alloy had a better corrosion resistance than that of Ti–6Al–4V alloy in 0.9% NaCl solution. In addition, they studied

the corrosion behaviors of Ti–5Al–2Nb–1Ta alloys in Hank's solution at different immersion periods [18]. *Popa* et al. [19] have correlated the microstructure with the corrosion resistance for Ti–6Al–7Nb alloy with different thermo-mechanical processing in Ringer's solution. The thermo-mechanical processing improved the electrochemical behavior of Ti–6Al–7Nb alloys, especially their passive state. *Lopez* et al. [20] have carried out a comparative study on the corrosion behaviors of Ti–6Al–7Nb, Ti–13Nb–13Zr, and Ti–15Zr–4Nb alloys in Hank's solution and they have reported very similar current densities for all the three titanium alloys. *Assis* and *Costa* [21] have reported a slightly improved corrosion resistance associated to the Ti–13Nb–13Zr and Ti–6Al–7Nb alloys compared to the Ti–6Al–4V alloy. *Robin* et al. [22] studied the corrosion behavior of Ti–xNb–13Zr alloys in Ringer's solution. There was evidence that the Ti–xNb–13Zr alloys were more corrosion resistant than both Ti and Ti–6Al–4V in Ringer's solution. The resistance of the passive film decreased with increasing the Nb contents. *Martins* et al. [23] have studied the corrosion resistance of Ti–30Nb–Zr casting alloy. Zirconium, as a β isomorphous element, which belongs to the same group with titanium in the periodic table of elements, shows complete mutual solubilities in both α and β structured titanium phases. The effect of the Zr element on the corrosion resistance should be studied clearly.

The aim of the present study was to investigate the effect of Zr addition on the electrochemical corrosion behavior of the Ti–22Nb alloy in 0.9% NaCl solution at 37 °C and neutral pH range. Furthermore, the variation of the corrosion behaviors of these alloys before and after potentiodynamic polarization, when exposed to aggressive Cl$^-$ environment, was also investigated.

2 Materials and methods

The Ti–22Nb and Ti–22Nb–6Zr (6 at%) alloy samples were prepared by arc-melting method using pure Ti (99.99%), pure Nb (99.99%), and pure Zr (99.99%) with non-consumable W electrode. To ensure the homogeneity, the ingots were re-melted five times. Then they were cold-rolled to plates of ~1 mm in thickness with the final cold working ratio of ~90%. The cold-rolled plates were finally solution-treated at 900 °C for half an hour and quenched into iced water. All the samples were prepared by electro-discharge machining from the solution-treated plates. Surfaces of the samples were mechanically polished with waterproof silicon carbide paper down to 2000 grade. Before electrochemical test, all the samples were cleaned using acetone, ethanol, and de-ionized water in an ultrasonic bath for 15 min and then dried in air. X-ray diffraction (XRD) patterns were obtained utilizing a Philip X'Pert Pro diffractometer operated at 40 kV and 40 mA, with a Ni-filtered Cu Kα radiation and a wavelength, λ, of 1.5406 nm.

The electrochemical experiments were performed in a traditional three-electrode cell. The sample, a platinum electrode, and a saturated calomel electrode (SCE) were used as a working electrode, a counter electrode, and a reference electrode, respectively. The electrolyte was 0.9% NaCl solution with neutral pH value, made up with laboratory-grade chemicals and de-ionized water. All experiments were carried out at 37 °C. The electrochemical parameters were controlled through a Solartron

1287 potentiostat combined with a Solartron 1260 frequency response analyzer.

The open circuit potential (OCP) measurements were done for 1 h in 0.9% NaCl electrolyte before and after polarization. The potentiodynamic polarization curves of the test samples were measured from −0.6 V (*vs.* SCE) to about 1.5 V (*vs.* SCE) with a scan rate of 1 mV/s after keeping the alloy electrodes at OCP for 1 h. The corrosion potential (E_{corr}) and the corrosion current density (I_{corr}) were obtained by Tafel analysis based on the polarization plots. The variations of the corrosion behavior for the passive film formed on the surface of the samples before and after potentiodynamic polarization were studied using electrochemical impedance spectroscopy (EIS) technique. The impedance spectra were acquired in the frequency range of 10^4–10^{-2} Hz with a 10 mV amplitude sine wave at OCP. To obtain the quantitative information for the discussions of theses experimental EIS results, the appropriate models (Zview2 version) for equivalent circuit quantification were used.

3 Results and discussion

3.1 Microstructures

Figure 1 shows the XRD patterns of the solution-treated Ti–22Nb and Ti–22Nb–6Zr alloy samples measured at room temperature. Besides the β phase peaks, the obvious diffraction peaks of α''(110), α''(200), and α''(113) for the Ti–22Nb alloy sample are observed, as shown in Fig. 1. In contrast, the solution-treated Ti–22Nb–6Zr alloy sample is only composed of single β phase, as shown in Fig. 1. It has been reported in the literature that the amount of α'' martensite decreases with an increase in the β stabilizing elements content during the quenching process [24–28]. When the Nb content overruns a constant value, the β phase can be retained for the β titanium alloy quenched from the β phase. From Fig. 1, it can also be seen that the addition of Zr suppresses the precipitation of the metastable α'' martensitic phase and stabilizes the β phase during the quenching process, as reported in the literature [23, 29, 30]. Typical optical micrograph of the solution-treated Ti–22Nb alloy sample is shown in Fig. 2(a).
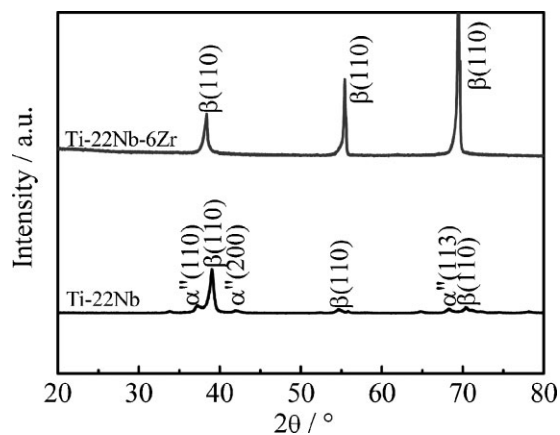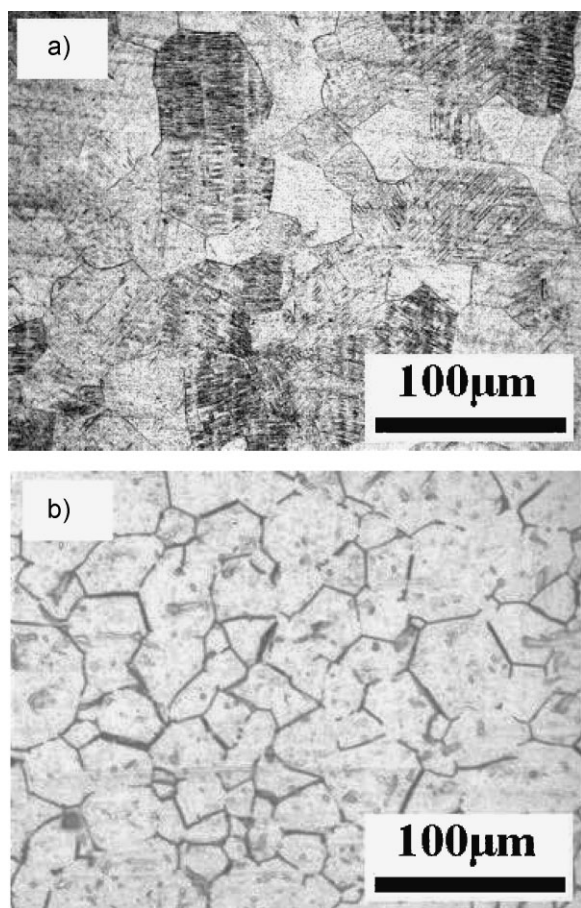

Figure 1. XRD patterns for the Ti–22Nb and Ti–22Nb–6Zr alloy samples (900 °C, 30 min, WQ)
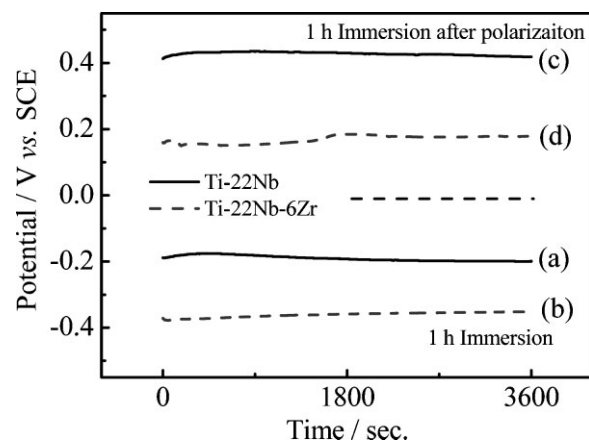
The samples exhibits an acicular martensite α'' phase disseminated in the β matrix, as identified by the XRD patterns, shown in Fig. 1. Because of the introduction of α'' martensite, the remaining β matrix becomes enriched in β stabilizing elements and somewhat depleted in α stabilizing elements, which induced an uneven distribution of the alloying elements. However, the Ti–22Nb–6Zr alloy sample exhibits an equiaxial β grain with the even distribution of the alloying elements, as shown in Fig. 2(b). The effect of the observed phase to the corrosion behavior of these two alloys will be discussed later.

3.2 Open circuit potential (OCP)

Figure 3 presents the variations of OCP for the Ti–22Nb and Ti–22Nb–6Zr alloy samples as a function of exposure time in 0.9% NaCl before and after potentiodynamic polarization. Every curve indicates a passivation. The OPCs reach to the stable values after 1 h exposure in 0.9% solution, which means the passive films become stable. From these curves, it can be seen that the samples polarized in 0.9% NaCl solution have higher OPC values than those immersed in the solution before polarization. *Yu* et al. have reported an increase in thickness of the oxide film with the potential, which play an important role in the improvement of the corrosion resistance [31]. Uniform surface corrosion of Ti–Nb or

Figure 3. Plots of OCP *versus* time for the Ti–22Nb and Ti–22Nb–6Zr alloy samples in 0.9% NaCl solution

Ti–Nb–Zr alloys provides a passive film that is mainly formed by TiO_2, Nb_2O_5, or ZrO_2 [14, 15, 32]. Compared to the film spontaneously formed in air, the polarization leads to a complete transformation from TiO or Ti_2O_3 to TiO_2 (more stable) over 1.2 V (*vs.* SCE), which is helpful for improvement of corrosion resistance [33]. The higher OCP values for the polarized samples should be attributed to the potentiodynamic polarization.

3.3 Potentiodynamic polarization studies

Figure 4 shows the potentiodynamic polarization plots for the Ti–22Nb and Ti–22Nb–6Zr alloy samples after 1 h immersion in 0.9% NaCl solution. The corrosion potentials (E_{corr}) were −0.307 and −0.442 V (*vs.* SCE) estimated from these curves for the Ti–22Nb and Ti–22Nb–6Zr alloy samples, respectively. The corrosion current densities (I_{corr}) were obtained from the polarization curves by Tafel analysis using both anodic and cathodic branches of the polarization curves, as shown in Fig. 4. The corrosion current density for the Ti–22Nb alloy sample is ∼0.633 µA/cm². However, the Ti–22Nb–6Zr alloy sample is only about 0.026 µA/cm², which is much lower than that of Ti–22Nb alloy sample. It is clear that the corrosion current density for the Ti–22Nb–6Zr alloy

Figure 2. Typical optical micrographs for the solution-treated Ti–22Nb and Ti–22Nb–6Zr alloy samples.
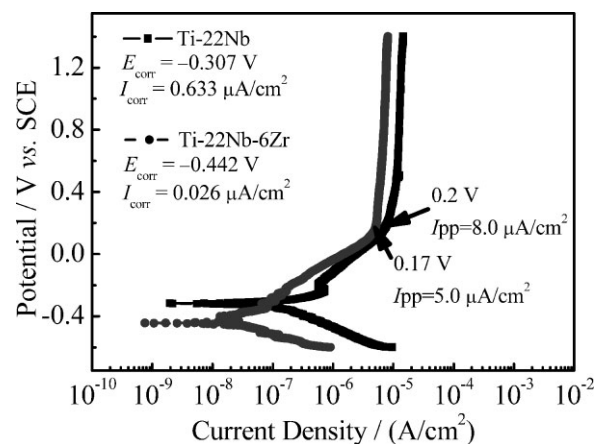
Figure 4. Potentiodynamic polarization curves for the Ti–22Nb and Ti–22Nb–6Zr alloy samples in 0.9% NaCl solution

sample becomes lower because of the addition of Zr element. Such results agree well with the experimental results obtained by *Martins* et al. [23]. Therefore, the addition of Zr reinforces the corrosion-resistant tendency for the Ti–22Nb alloy.

From Fig. 4, it can be seen that the two samples exhibit a self-passivated characterization, translating directly into the passive region from the Tafel region. These oxide films become stable at 0.20 and 0.17 V (*vs.* SCE) for the Ti–22Nb and Ti–22Nb–6Zr alloy samples, respectively. No breakdown potential is observed in the range of potential test (until to ∼1.5 V *vs.* SCE), which indicates that these passive films formed on the surface of these titanium alloys are very integral and protective, thus preventing corrosion [34, 35]. Different passive current densities (I_{pp}) are associated to such corrosion potential for each alloy. Higher I_{pp} is exhibited by the Ti–22Nb alloy sample, which is about 8.0 μA/cm^2. The I_{pp} value for the Ti–22Nb–6Zr alloy sample is about 5.0 μA/cm^2. The association of values of I_{corr} and I_{pp} permits to conclude that the Ti–22Nb–6Zr alloy has a nobler electrochemical behavior when compared to the Ti–22Nb binary alloy.

3.4 Electrochemical impedance spectrum (EIS) analysis

To make clear the effect of Zr addition and polarization on the electrochemical behavior, EIS was performed for the alloys in 0.9% NaCl solution. Figure 5 shows the experimental and the simulated EIS results for the two alloy samples immersed in 0.9% NaCl solution for 1 h. The Nyquist plots and Bode plots are characterized by similar behavior in nature for these two samples. In Fig. 5(a), it is obvious that all the Nyquist plots in the impedance spectra are characterized by a large depressed semicircle and the diameter of the semicircle becomes larger with the addition of Zr, which indicates a nobler electrochemical behavior [36] for the Ti–22Nb–6Zr alloy. From the Bode-magnitude plots shown in Fig. 5(b), it can be seen that there are two distinct regions for these two samples immersed 1 h in 0.9% NaCl solution. In the high frequency (1–100 kHz), a flat portion of curves (slope ≈ 0) is observed due to the response of electrolyte. In the low- and middle-frequency ranges, the impedance spectrum displays a linear slope of about −1, which is the characteristic response of a capacitive behavior of passive film [37–39]. There are three characteristic regions in the Bode-phase plots in Fig. 5(b). In the high-frequency range, the phase angle drops to 0° with the response of electrolyte resistance; in the middle frequency, the phase angle remains near to −75° indicating a typical passive film presented on the surface and a near capacitive response for passive film; and in the low frequency, the phase angle decreases to lower value because of the contribution of the passive film resistance [37–39]. It should be noted that the frequency range over the phase angle of close to −75° and the maximum phase angle increase with the addition of Zr, which indicates the reinforcement of ''ideal'' capacitive behavior of the passive film. Higher impedance and phase angle are conducive to a nobler electrochemical behavior [40, 41]. The addition of Zr element is helpful to increase the resistance of the passive film for the Ti–22Nb alloy sample in 0.9% NaCl solution.

Figure 6 shows the experimental and simulated EIS results for the two alloy samples which have been polarized in 0.9% NaCl solution. Compared with the impedance spectra of the two samples
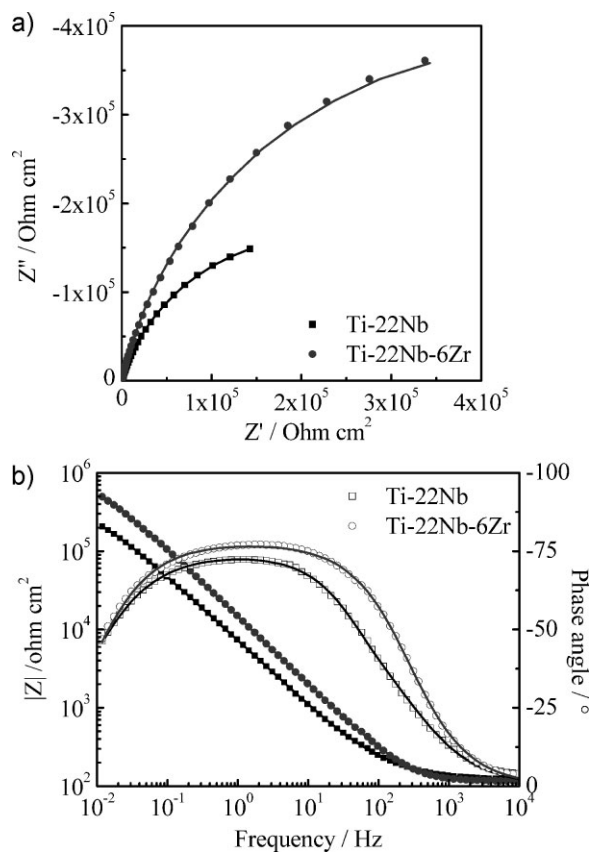

Figure 5. Electrochemical impedance spectra of the Ti–22Nb and Ti–22Nb–6Zr alloy samples after 1 h immersion in 0.9% NaCl. (a) Nyquist plots and (b) Bode plots. (Line: fitted data; symbol: experimental data.)

without polarization (after 1 h immersion), distinct spectra are observed. In the case of the polarization, the Nyquist plots, as seen in Fig. 6(a), show two relaxation time constants. This is also indicated by the two peaks in the Bode-phase plots, as represented in Fig. 6(b). These behaviors evince the formation of a duplex film for each of the two alloy samples after polarization in 0.9% NaCl solution. After polarization, significant displacements on the modulus of impedance for these two alloy samples have been clearly observed. It seems that after polarization, the passive oxide film is better protective than that after 1 h immersion.

According to the EIS results obtained for the two alloy samples after 1 h immersion, the $R_s(Q_pR_p)$ model with only one time constant as shown in Fig. 7(a), was used as the equivalent circuit model to fit the EIS data in the case of single passive film present on the metal surface, as shown in Fig. 5. R_s is the electrolyte resistance. R_p is the resistance of passive film. Q_p is the constant phase element. The proposed equivalent circuit model shown in Fig. 7(a) is widely used for the fit of a single film on the surface of titanium alloys [37–39, 42–45]. For these two polarized samples, the $R_s(Q_o(R_o(Q_bR_b)))$ model, shown in Fig. 7(b), was used to fit the EIS data, as shown in Fig. 6. The physical significance of the circuit elements for this model has been reported in the literature [23, 28, 46–49]. The duplex film is composed of a dense inner barrier layer (bL) and a porous outer layer (oL). R_s corresponds to the electrolyte resistance. R_o and R_b
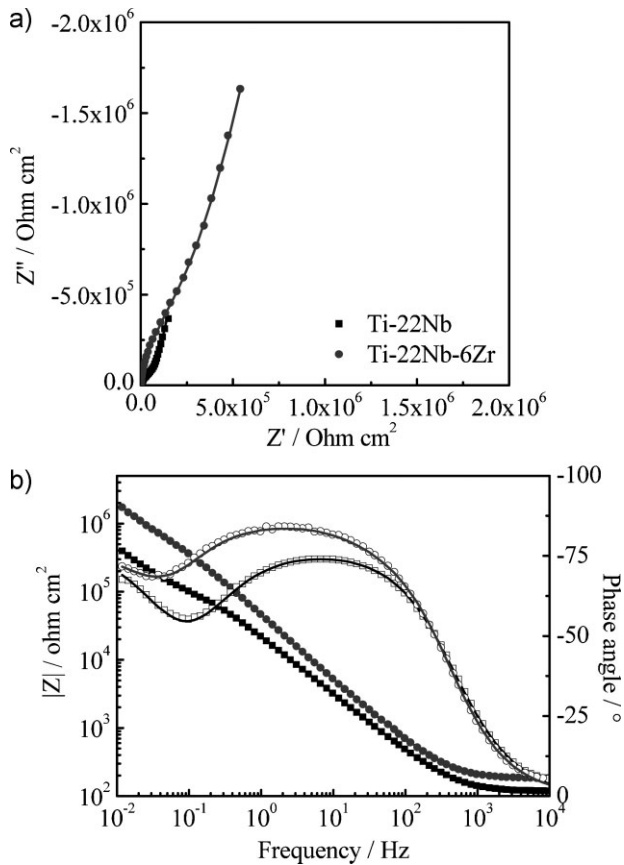
Figure 6. Electrochemical impedance spectra of the Ti–22Nb and Ti–22Nb–6Zr alloy samples after polarization in 0.9% NaCl. (a) Nyquist plots and (b) Bode plots. (Line: fitted data; symbol: experimental data.)
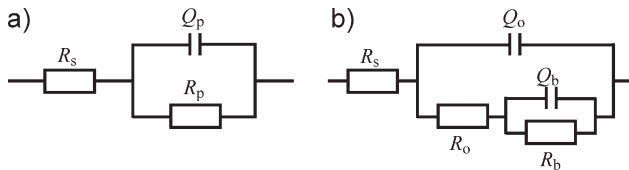
Figure 7. Models used to fit the EIS data: (a) $R_s(Q_pR_p)$ model and (b) $R_s(Q_o(R_o(Q_bR_b)))$ model

are the resistances of outer and inner layers. Q_o and Q_b are defined as capacitances of outer and inner layers.

All the parameters fitted by the two models are listed in Tables 1 and 2 for the two alloy samples after 1 h immersion before and after polarization in 0.9% NaCl solution, respectively. The good agreement between the experimental data and fitted data is obtained with the χ^2 of about 10^{-4}. As shown in Table 1, comparison between the capacitance (Q_p) and the resistance (R_p)

Table 1. Values of fitting parameters obtained using the $R_s(Q_pR_p)$ model to fit the experimental EIS data for the Ti–22Nb and Ti–22Nb–6Zr alloy samples after 1 h immersion

Alloys	R_s (Ω/cm^2)	Q_p (μF/cm^2)	n	$R_p \times 10^5$ (Ω/cm^2)	χ^2
Ti–22Nb	126.9	30.8	0.82	4.4	1.7×10^{-4}
Ti–22Nb–6Zr	113.5	14.0	0.86	9.3	2.9×10^{-4}

of the passive films for the Ti–22Nb and Ti–22Nb–6Zr alloy samples after 1 h immersion, permit to observe that the latter has a lower capacitance ($\sim$14.0 μF/cm^2) and higher resistance ($\sim$9.3 $\times 10^5$ Ω/cm^2) than those of the former. This indicates that the Ti–22Nb–6Zr alloy has a nobler electrochemical corrosion behavior when compared to the Ti–22Nb alloy. The same conclusion can be drawn for the two alloys after polarization in 0.9% NaCl solution, as shown in Table 2. The polarized Ti–22Nb–6Zr alloy sample shows the higher R_o and R_b and lower Q_o and Q_b and has a nobler electrochemical corrosion behavior compared to the polarized Ti–22Nb alloy sample. In addition, the inner film of the two polarized alloy samples exhibits a much larger resistance compared to the outer film. These results suggest that the corrosion protection is dominated by the inner layer. On the other hand, the porous outer layer is helpful for the osseointegration between implant and human bone [23]. Comparing the EIS results of the samples before and after polarization, the R_o and R_b for the samples after polarization increase much higher compared with those of the two samples before polarization. These impedance parameters permit to conclude that both inner and outer layers can provide a better corrosion protection when compared to the samples with a single film. So, the polarization improves the corrosion resistance for titanium alloys. As reported by *Yu* et al. [31], the thickness of the oxide film increases with applied potential. *Martins* et al. have reported the increase in the thickness of the oxide films and/or the oxide density of the inner barrier layer [23]. The same results have recently reported that the corrosion rates decreased due to a thicker oxide film formation by potentiodynamic polarization in the Ti–Nb binary alloy [28]. Generally speaking, the corrosion resistance of Ti alloy systems can be largely improved by the addition of Zr and the polarization.

3.5 Relationship of the microstructures with the electrochemical corrosion behavior

Experimental results of EIS and polarization measurements associated to an equivalent circuit analysis have shown that the alloying element can be used to alternate the resulting microstructure which affects the electrochemical behavior of titanium alloy. In the present investigation, the results of corrosion tests have indicated that the Ti–22Nb–6Zr alloy sample

Table 2. Values of fitting parameters obtained using the $R_s(Q_o(R_o(Q_bR_b)))$ model to fit the experimental EIS data for the Ti–22Nb and Ti–22Nb–6Zr alloy samples after polarization in 0.9% NaCl solution

Alloys	R_s (Ω/cm^2)	Q_o (μF/cm^2)	n_o	$R_o \times 10^5$ (Ω/cm^2)	Q_b (μF/cm^2)	n_b	$R_b \times 10^6$ (Ω/cm^2)	χ^2
Ti–22Nb	115.5	9.2	0.85	1.8	17	0.90	24	4.7×10^{-4}
Ti–22Nb–6Zr	185	4.0	0.92	20.1	3.7	1	192	4.3×10^{-4}

has a nobler electrochemical behavior compared to that of the Ti–22Nb alloy sample. The Ti–22Nb alloy results in a microstructure formed by an acicular martensitic α'' phase in a β matrix, while the Ti–22Nb–6Zr alloy results in a microstructure consisting only β phase, as shown in Fig. 2. As mentioned previously, the β matrix is enriched in the β-stabilizing elements and exhibits a nobler characteristic. However, the α'' martensite is enriched in α-stabilizing elements and is a less noble acicular phase. The micro cell galvanic corrosion may be induced to decrease the corrosion resistance of the Ti–22Nb alloy. On the other hand, the Ti–22Nb–6Zr alloy has a microstructure formed by a homogeneous β phase without the occurrence of the aforementioned deleterious effects. In addition, the Ti, Nb, and Zr elements are solution-treated in the Ti–22Nb–6Zr alloy and the alloying elements are evenly distributed, which is helpful in the formation of the passive film with homogeneous chemical composition and can provide a superior corrosion resistance compared to the uneven distribution of the alloying elements in the Ti–Nb alloy [50].

4 Conclusions

On the basis of the above discussion, the main conclusions can be summarized as such:

The Ti–22Nb alloy sample is composed of β + α'' phases at room temperature. However, the Ti–22Nb–6Zr alloy sample is composed of single β phase at room temperature. It means that the addition of Zr stabilizes the β phase and suppresses the precipitation of α'' phase.

The EIS results of the immersed and polarized samples can be well fitted using the models of $R_s(Q_pR_p)$ and $R_s(Q_o(R_o(Q_bR_b)))$, respectively. This indicates different structures of passive films formed on the surfaces of the immersed and polarized alloy samples.

The association of values of I_{pp}, I_{corr}, and impedance parameters indicates that the electrochemical corrosion behavior of the Ti–22Nb alloy has been improved by the addition of Zr for it could induce the microstructure changes for Ti–22Nb alloy and results in an even distribution of alloying elements.

The potentiodynamic polarization can significantly improve the electrochemical corrosion behavior of the titanium alloys compared to the immersion samples.

5 References

[1] D. M. Brunette, P. T. M. Textor, P. Thomsen, *Titanium in Medicine*, Springer, Berlin, Heidelberg, New York **2001**.

[2] S. Rao, T. Ushida, T. Tateishi, Y. Okazaki, S. Asao, *Biomed. Mater. Eng.* **1996**, 6, 79.

[3] P. R. Walker, J. Leblanc, M. Sikorska, *Biochemistry* **1989**, 28, 3911.

[4] B. Sarkar, *Biological Aspects of Metals and Metal-Related Disease*, Raven Press, New York **1983**, pp. 209–218.

[5] D. Summer, J. Gatahte, *Clin. Orthop. Relat. Res.* **1992**, 274, 202.

[6] D. J. Lin, C. C. Chuang, J. H. C. Lin, J. W. Lee, C. P. Ju, H. S. Yin, *Biomaterial* **2007**, 28, 2582.

[7] S. G. Steinemann, *Surface Performance of Titanium*, TMS, Warrendale, Pennsylvania **1996**, p. 33.

[8] K. Wang, L. Gustavson, J. Dumbleton, *Beta Titanium in the 1990s*, TMS, Warrendale, Pennsylvania **1993**, pp. 2697–2710.

[9] M. Niinomi, *J. Mech. Behav. Biomed. Mater.* **2008**, 1, 30.

[10] Y. L. Hao, S. J. Li, S. Y. Sun, C. Y. Zheng, R. Yang, *Acta Biomater.* **2007**, 3, 277.

[11] S. G. Steinemann, P. A. Mausli, S. Szmuklermoncler, M. Emlitsch, O. Pohler, H. E. Hintermann, *Beta Titanium in the 1990s*, TMS, Warrendale, Pennsylvania **1993**, pp. 2689–2696.

[12] M. V. Popa, I. Demetrescu, D. Iordachescu, A. Cimpean, E. Vasilescu, P. Drob, C. Vasilescu, M. Istratescu, *Mater. Corros.* **2007**, 58, 687.

[13] Z. Cai, T. Shafer, I. Watanabe, M. E. Nunn, T. Okabe, *Biomaterial* **2003**, 24, 213.

[14] Y. F. Zheng, B. L. Wang, J. G. Wang, C. Li, L. C. Zhao, *Mater. Sci. Eng.* **2006**, 438A, 891.

[15] M. Anuwar, R. Jayaganthan, V. K. Tewari, N. Arivazhang, *Mater. Lett.* **2007**, 61, 1483.

[16] D. Mareci, G. Ungureanu, D. M. Aelenei, J. C. Mirza Rosca, *Mater. Corros.* **2007**, 58, 848.

[17] S. Tamilselvi, R. Murugaraj, N. Rajendran, *Mater. Corros.* **2007**, 58, 113.

[18] S. Tamilselvi, N. Rajendran, *Mater. Corros.* **2007**, 58, 285.

[19] M. V. Popa, D. Raducanu, E. Vasilescu, P. Drob, D. Cojocaru, C. Vasilescu, S. Ivanescu, J. C. Mirza Rosca, *Mater. Corros.* **2008**, 59, 919.

[20] M. F. Lopez, A. Gutierrez, J. A. Jimenez, *Electrochim. Acta* **2002**, 47, 1359.

[21] S. L. Assis, I. Costa, *Mater. Corros.* **2007**, 58, 329.

[22] A. Robin, O. A. S. Carvalho, S. G. Schneider, S. Schneider, *Mater. Corros.* **2008**, 59, 929.

[23] D. Q. Martins, W. R. Osório, M. E. P. Souza, R. Caram, A. Garcia, *Electrochim. Acta* **2008**, 53, 2809.

[24] R. Godley, D. Starosvetsky, I. Gotman, *J. Mater. Sci.: Mater. Med.* **2006**, 17, 63.

[25] T. Ahmed, H. J. Rack, *J. Mater. Sci.* **1996**, 31, 4267.

[26] Y. Mantani, M. Tajima, *Mater. Sci. Eng.* **2006**, 438A, 315.

[27] H. Y. Kim, Y. Ikehara, J. I. Kim, H. Hosoda, S. Miyazaki, *Acta Mater.* **2006**, 54, 2419.

[28] A. Cremasco, W. R. Osório, C. M. A. Freire, A. Garcia, R. Caram, *Electrochim. Acta* **2008**, 53, 4867.

[29] J. I. Kim, H. Y. Kim, T. Inamura, H. Hosoda, S. Miyazaki, *Mater. Sci. Eng.* **2005**, 403A, 334.

[30] H. F. Mohamed Abdel-Hady, K. Hinoshita, H. Kimura, Y. Shinzato, M. Morinaga, *Scr. Mater.* **2007**, 57, 1000.

[31] S. Y. Yu, J. R. Scully, *Corrosion* **1997**, 53, 965.

[32] N. T. C. Oliveira, S. R. Biaggio, P. A. P. Nascente, R. C. Rocha-Filho, N. Bocchi, *Surf. Interface Anal.* **2006**, 38, 410.

[33] S. L. Assis, S. Wolynec, I. Costa, *Electrochim. Acta* **2006**, 51, 1815.

[34] P. Kovacs, *Trans. Soc. Biomater.* **1993**, 19, 272.

[35] R. J. Solar, S. R. Pollack, E. Korostoff, *J. Biomed. Mater. Res.* **1979**, 13, 217.

[36] Y. Z. Huang, D. J. Blackwood, *Electrochim. Acta* **2005**, 51, 1099.

[37] E. G. Gonzalez, J. C. Mirza-Rosca, *J. Electroanal. Chem.* **1999**, 471, 109.

[38] A. K. Shukla, R. Balasubramaniam, S. Bhargava, *Intermetallics* **2005**, 13, 631.

[39] A. W. E. Hodgson, Y. Mueller, D. C. Forster, S. Virtanen, *Electrochim. Acta* **2002**, *47*, 1913.

[40] W. R. Osorio, P. R. Goulart, G. A. Santos, C. M. Neto, A. Garcia, *Metall. Mater. Trans.* **2006**, *37A*, 2525.

[41] W. R. Osorio, J. E. Spinelli, I. L. Ferreira, A. Garcia, *Electrochim. Acta* **2007**, *52*, 3265.

[42] S. Tamilselvi, V. Raman, N. Rajendran, *Electrochim. Acta* **2006**, *52*, 839.

[43] H. H. Huang, *Electrochim. Acta* **2002**, *47*, 2311.

[44] M. Karthega, V. Raman, N. Rajendran, *Acta Biomater.* **2007**, *3*, 1019.

[45] F. Laurent, B. Grosgogeat, L. Reclaru, F. Dalard, M. Lissac, *Biomaterials* **2002**, *22*, 2273.

[46] J. Pan, D. Thierry, C. Leygraf, *Electrochim. Acta* **1996**, *41*, 1143.

[47] S. Gudic, J. Radosevic, M. Kliskic, *Electrochim. Acta* **2002**, *47*, 3009.

[48] W. R. Osorio, J. E. Spinelli, N. Cheung, A. Garcia, *Mater. Sci. Eng.* **2006**, *420A*, 179.

[49] W. R. Osorio, N. Cheung, J. E. Spinelli, P. R. Goulart, A. Garcia, *J. Solid State Electrochem.* **2007**, *11*, 1421.

[50] M. Geetha, U. Kamachi Mudali, A. K. Gogia, R. Asokamani, Raj. Baldev, *Corros. Sci.* **2004**, *46*, 877.